Supplement of Atmos. Chem. Phys., 22, 9199–9213, 2022
https://doi.org/10.5194/acp-22-9199-2022-supplement

Atmospheric Chemistry and Physics
Open Access
EGU

Supplement of

Light absorption by brown carbon over the South-East Atlantic Ocean

Lu Zhang et al.

Correspondence to: Lu Zhang (luzhang@mail.tau.ac.il), Michal Segal-Rozenhaimer (msegalro@tauex.tau.ac.il)

S1 Optical models

Four different optical models are used in this study: the core-shell (CS) Mie model and three homogeneous grey sphere models – the volume mixing (VM) model, Maxwell-Garnett (MG) model, and Bruggeman (BG) model.

i) The core-shell (CS) model assumes the BC core is concentrically located inside non-BC materials, i.e. the shell. Inputs of the CS model are the refractive indices of both the core and shell and the 2-D BC size and mixing state (i.e., coating thickness) distribution.

ii) For the homogeneous grey sphere models, inputs are the PNSD and effective refractive index. The three mixing rules that were used to compute the effective refractive index ($m_{eff} = n+ki$) are:

   a) The volume mixing (VM) rule, which assumes components are well mixed within the particle. Similar to the calculation of bulk density, the effective refractive index (m_{eff}) is calculated following the volume mixing rule:

$$m_{eff} = \sum_i f_i m_i \quad (1)$$

   where f_i is the volume fraction of component i, and m_i is the refractive index of component i.

   b) The Maxwell-Garnett (MG) mixing rule assumes an inclusion (BC in our case) with permittivity ε_1 and volume fraction f_1 is embedded within a host medium (non-BC materials) with permittivity ε_2. The effective permittivity can be computed as (Bohren and Huffman, 2008):

$$\epsilon = \frac{\epsilon_1 + 2\epsilon_2 + 3f_1(\epsilon_1 - \epsilon_1)}{\epsilon_1 + 2\epsilon_2 - f_1(\epsilon_1 - \epsilon_2)} \quad (2)$$

   The refractive index is the square root of the permittivity:

$$m = \sqrt{\epsilon} \quad (3)$$

   c) The Bruggemann (BG) mixing rule is derived from the same base equation as the Maxwell-Garnett mixing rule, while using a different approximation. It assumes two inclusions embedded within a host matrix with a permittivity (Markel, 2016):

$$\epsilon = \frac{1}{4}(b + \sqrt{8\epsilon_1\epsilon_2 + b^2}) \quad (4)$$

$$b = 3f_1(\epsilon_1 - \epsilon_2) + 2\epsilon_2 - \epsilon_1 \quad (5)$$

   It treats the two components more symmetrically.

For BC-containing particles, f_1 represents the volume fraction of BC, which can be calculated from BC 2-D size and mixing state distributions determined by the SP2.

S2 Evaluation of the assumption of zero absorption of BrC at 660 nm

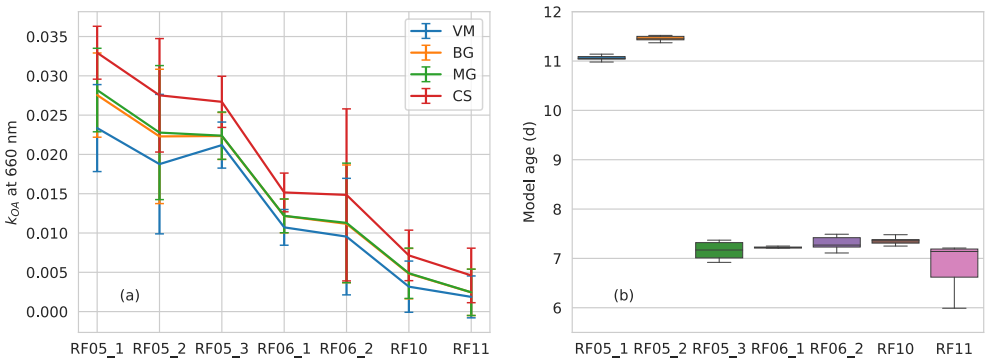

Figure. S1 (a) The imaginary refractive index k_{OA} at 660 nm and (b) the aerosol/plume age for each flight. The aerosol/plume age was modelled with a two-week forecast using the Weather Research and Aerosol Aware Microphysics (WRF-AAM) model.

To support our assumption of negligible BrC absorption at 660 nm, we assumed the absorption not attributed to BC at 660 nm to be solely from OA, and calculated the imaginary part of the refractive index of OA, k_{OA}, at 660 nm with different the VM, BG, MG, and CS models, following the method in Liu et al. (2021). A refractive index of BC of 1.95+0.79i was used, which is an upper bound of commonly used BC refractive index and thereby yields an upper bound of BC absorption and a lower bound of BrC absorption. The real refractive index of OA was set to be 1.55. Results of k_{OA} at 660 nm are shown in Fig. S2. The k_{OA} at 660 nm is lowest for particles in RF11, the least aged with the aerosol/plume age of 6.8±0.4 days, and highest for RF05_1 and RF05_2, the most aged with the aerosol/plume age greater than 11 days. The increase of k_{OA} for more aged aerosols seems to be in inconsistent with the fact that BrC experiences photolysis and photochemical bleaching during transport, which will thereby lessen its absorbance considerably (Laskin et al., 2015). Aqueous-phase aging may form light-absorbing oligomeric products, while we observe no obvious differences in the liquid water content during the transport of investigated flights. Furthermore, higher absorptivity of BrC is associated with an increase in molecular size and decrease in volatility (Saleh et al., 2018), therefore, more aged particles that tends to exhibit higher volatility in this study (Dang et al., 2021) are expected to show lower absorptivity than less aged ones, which is again inconsistent with the increase of k_{OA} for more aged aerosols as shown in Fig. 1. Both the aging time and volatility challenges the counter-assumption that absorption at 660 nm is contributed solely by BrC except for BC; hence, we conclude that other absorbers are expected to exist.

We took the k_{OA} of the least aged particles in RF11 as the upper limit of k_{OA} for all flights and used it to calculate the m_{eBC} and absorption coefficients of BrC at 660 nm. Results showed that the difference between the BrC absorption coefficients with k_{OA} of RF11 and those calculated with the assumption of non-absorbing OA at 660 nm is smaller than 9 % for the extreme case of RF10 with the thickest coating. Therefore, we neglected the possible contribution of BrC at 660 nm in the retrieval of m_{eBC}.

S3 Uncertainty analysis

The uncertainty of the imaginary part of the effective refractive index of BC (k_{eBC}) and absorption coefficients calculated with m_{eBC} and m_{BC} of 1.95+0.79i at 470, 530, and 660 nm ($\sigma_{abs,eBC}$ and $\sigma_{abs,BC}$) were estimated using the Monte Carlo uncertainty analysis. It is applied because of the complexity of the retrieval process of k_{eBC} and the calculation of $\sigma_{abs,BrC}$ and $\sigma_{abs,eBC}$. The uncertainty of absorption coefficients of BrC at 470 and 530 nm ($\sigma_{abs,470,BrC}$ and $\sigma_{abs,530,BrC}$), the mass absorption cross section of OA at 470 nm ($MAC_{OA,470}$), and the contribution of BrC to the total absorption at 470 nm ($R_{BrC,470}$) were then calculated analytically.

Following the approach in Taylor et al. (2020), we used the uncertainty in each input variable to generate an array of scale factors to represent the variability of the variable may have when measured a large number of times. Specifically, we first generated an array of scale factors that follows the Gaussian distribution with a mean of 1 and a standard deviation of the uncertainty for each input variable. The array of scale factors was then multiplied by the corresponding input variable to generate an array of variables, representing the possibility of this input variable if it were measured a large number of times, 10000 is used in this study. Variables considered in this analysis include the BC core size distribution, BC coating thickness, absorption coefficients, and OA mass concentration (Fischer et al., 2010). For the BC coating thickness and OA mass concentration, we used the conservative value of 2-σ uncertainty (Bahreini et al., 2009; Taylor et al., 2020). Input variables and corresponding uncertainties are shown in Table S1. An uncertainty of 4% was given to the real part of refractive index of the coating following Taylor et al. (2020).

Table S1. Uncertainty of input variables of the Monte-Carlo uncertainty analysis, corresponding instruments were also given.

	Uncertainty	Instrument
BC core mass	20%	SP2
Coating thicknesses	22%	SP2
Measured absorption coefficients	20%	PSAP
OA mass	38%	AMS

The results of uncertainty analysis are shown in Table S2. The uncertainties from VM, MG, and BG models are very close. The uncertainty of k_{eBC} obtained from homogeneous models and the CS model was 24 % and 35 %, respectively. The uncertainty of $R_{BrC,470}$ and $MAC_{OA,470}$ was ~35% and 48%, respectively. The high uncertainty of $MAC_{OA,470}$ mainly results from the large uncertainty of OA mass measured by the AMS. All MAC_{OA} would be subject to this large uncertainty if the OA mass was determined by AMS.

Table S2. Monte Carlo relative standard deviations of k_{eBC}, $\sigma_{abs,eBC}$, and $\sigma_{abs,BC}$, and uncertainties of $\sigma_{abs,BrC}$, $R_{BrC,470}$, and $MAC_{OA,470}$ with different optical models.

	VM	MG	BG	CS
k_{eBC}	0.24	0.24	0.24	0.35
$\sigma_{abs,660,eBC}$	0.22	0.23	0.23	0.24
$\sigma_{abs,530,eBC}$	0.21	0.22	0.22	0.23
$\sigma_{abs,470,eBC}$	0.21	0.21	0.21	0.23
$\sigma_{abs,660,BC}$	0.56	0.56	0.56	0.51
$\sigma_{abs,530,BC}$	0.53	0.53	0.55	0.47
$\sigma_{abs,470,BC}$	0.51	0.51	0.51	0.45
$\sigma_{abs,530,BrC}$	0.29	0.30	0.30	0.30
$\sigma_{abs,470,BrC}$	0.29	0.29	0.29	0.30
$R_{BrC,470}$	0.35	0.35	0.35	0.36
$MAC_{OA,470}$	0.48	0.48	0.48	0.48

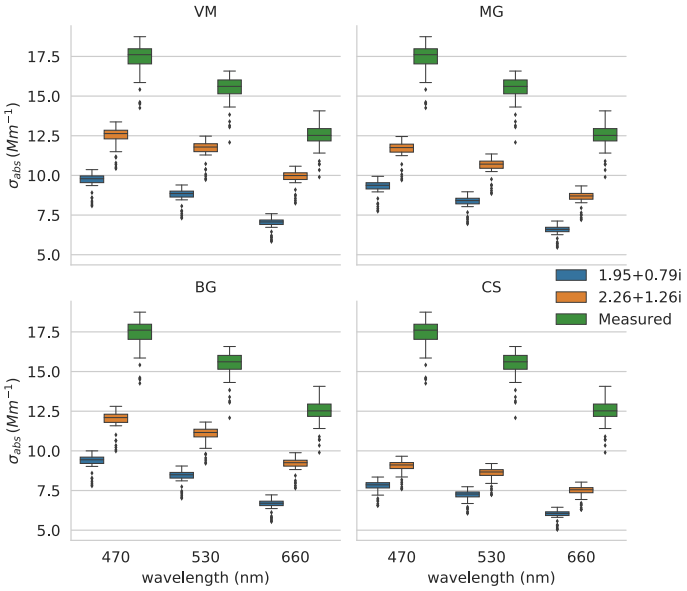

Figure S2. Modelled (blue and orange markers) and measured (green markers) absorption coefficients (σ_{abs}) at PSAP wavelengths for RF05_3. Variables are modelled with two m_{BC} values (shown in the legend) using the CS, MG, BG, and VM models (specified on the top of each plot). OA is assumed to be non-absorbing with the refractive index m_{OA} equal to 1.55+0i. The horizontal lines in the boxes represent the median value, the boxes represent 25th to 75th percentile, the whiskers represent 1.5 inter-quartile range, and the diamonds represent outliers.

References

Bahreini, R., Ervens, B., Middlebrook, A. M., Warneke, C., de Gouw, J. A., DeCarlo, P. F., Jimenez, J. L., Brock, C. A., Neuman, J. A., Ryerson, T. B., Stark, H., Atlas, E., Brioude, J., Fried, A., Holloway, J. S., Peischl, J., Richter, D., Walega, J., Weibring, P., Wollny, A. G., and Fehsenfeld, F. C.: Organic aerosol formation in urban and industrial plumes near Houston and Dallas, Texas, J. Geophys. Res. Atmospheres, 114, https://doi.org/10.1029/2008JD011493, 2009.

Bohren, C. F. and Huffman, D. R.: Absorption and Scattering of Light by Small Particles, John Wiley & Sons, 547 pp., 2008.

Dang, C., Segal-Rozenhaimer, M., Che, H., Zhang, L., Formenti, P., Taylor, J., Dobracki, A., Purdue, S., Wong, P.-S., Nenes, A., Sedlacek, A., Coe, H., Redemann, J., Zuidema, P., and Haywood, J.: Biomass burning and marine aerosol processing over the southeast Atlantic Ocean: A TEM single particle analysis, Atmospheric Chem. Phys. Discuss., 1–30, https://doi.org/10.5194/acp-2021-724, 2021.

Fischer, E. V., Jaffe, D. A., Marley, N. A., Gaffney, J. S., and Marchany-Rivera, A.: Optical properties of aged Asian aerosols observed over the U.S. Pacific Northwest, J. Geophys. Res. Atmospheres, 115, https://doi.org/10.1029/2010JD013943, 2010.

Liu, D., Li, S., Hu, D., Kong, S., Cheng, Y., Wu, Y., Ding, S., Hu, K., Zheng, S., Yan, Q., Zheng, H., Zhao, D., Tian, P., Ye, J., Huang, M., and Ding, D.: Evolution of Aerosol Optical Properties from Wood Smoke in Real Atmosphere Influenced by Burning Phase and Solar Radiation, Environ. Sci. Technol., 55, 5677–5688, https://doi.org/10.1021/acs.est.0c07569, 2021.

Markel, V. A.: Introduction to the Maxwell Garnett approximation: tutorial, JOSA A, 33, 1244–1256, https://doi.org/10.1364/JOSAA.33.001244, 2016.

Saleh, R., Cheng, Z., and Atwi, K.: The Brown–Black Continuum of Light-Absorbing Combustion Aerosols, Environ. Sci. Technol. Lett., 5, 508–513, https://doi.org/10.1021/acs.estlett.8b00305, 2018.

Taylor, J. W., Wu, H., Szpek, K., Bower, K., Crawford, I., Flynn, M. J., Williams, P. I., Dorsey, J., Langridge, J. M., Cotterell, M. I., Fox, C., Davies, N. W., Haywood, J. M., and Coe, H.: Absorption closure in highly aged biomass burning smoke, Atmospheric Chem. Phys., 20, 11201–11221, https://doi.org/10.5194/acp-20-11201-2020, 2020.